ChemPubSoc Europe

DOI: 10.1002/chem.201xxxxxx

CHEMISTRY
A European Journal
Full Paper

Ruthenium Complex

Synthesis and Single-Molecule Conductance Study of Redox Active Ruthenium Complexes with Pyridyl and Dihydrobenzo[b]thiophene Anchoring Groups

Hiroaki Ozawa,[a]Θ Masoud Baghernejad,[b]Θ Oday A. Al-Owaedi,*[c]Θ Veerabhadrarao Kaliginedi,*[b]Θ Takumi Nagashima,[a] Jaime Ferrer, [d] Thomas Wandlowski,[b] Víctor M. García-Suárez,[d] Peter Broekmann,[b] Colin J. Lambert[c] and Masa-aki Haga*[a]

Abstract: The ancillary ligands 4'-(4-pyridyl)-2,2':6',2''-terpyridine and 4'-(2,3-dihydrobenzo [b] thiophene)-2,2'-6',2"-terpyridine were used to synthesize two series of mono- and dinuclear ruthenium complexes differing in their lengths and anchoring groups. The electrochemical and single molecular conductance properties of these two series of ruthenium complexes were studied experimentally by means of cyclic voltammetry and the scanning tunnelling microscopy-break junction technique (STM-BJ) and theoretically by means of density functional theory (DFT). Cyclic voltammetry data showed clear redox peaks corresponding to both the metal and ligand related redox reactions. Single molecular conductance results demonstrated an exponential decay of the molecular conductance with the increase in molecular length for both the series of ruthenium complexes, with decay constants of β_{BT}= 2.07±0.1 and β_{PY} = 2.16±0.1, respectively. The contact resistance of complexes with 2,3-dihydrobenzo [b] thiophene (BT) anchoring groups is found to be smaller than the contact resistance of ruthenium complexes with pyridine (PY) anchors. DFT calculations support the experimental results and provided additional information on the electronic structure and charge transport properties in those metal/ruthenium complex/metal junctions.

Introduction

The understanding of conductance properties of metal/molecule/metal junctions has attracted wide attention because of their potential application as an alternative to silicon based technologies.[1] Hence, a variety of techniques have been developed to scrutinize the conductance of properties of metal/molecule/metal junctions, at a single-molecule level[2] (scanning tunnelling microscopy based break junctions (STM-BJ),[3] conducting probe atomic force microscopy break junction (CPAFM-BJ)[4] and mechanically controllable break junction technique (MCBJ))[5] and at the multi-molecular level[2a] (crossed wire junctions,[6] Gl-In eutectic based junctions,[7] Hg junctions[8] etc). By employing the above mentioned techniques, clear correlations between the molecular structure and the transport properties of molecular junctions could be derived for both single molecules and ensemble of molecules.[1a, 9] Therefore, organometallic complexes with metallic centers have attracted particular attention, as they often exhibit multi-trigger capabilities.

[a] Dr. H. Ozawa, T. Nagashima, Prof. M. Haga
Department of Applied Chemistry, Chuo University
1-13-27 Kasuga, Bunkyo-ku, 112-8551 Tokyo, Japan.
E-mail: mhaga@kc.chuo-u.ac.jp
[b] Dr. V. Kaliginedi, Dr. M. Baghernejad, Prof. P. Broekmann, Prof. Th. Wandlowski
Department of Chemistry and Biochemistry, University of Bern, Freistrasss3, CH-3012 Bern, Switzerland.
E-mail: kaliginedi@dcb.unibe.ch
[c] Mr.Oday A.Al-Owaedi,[⊥,#] Prof. Colin J. Lambert[#]
[#] Department of Physics, Lancaster University, Lancaster LA1 4YB, United Kingdom.
[⊥]Department of Laser Physics, Women Faculty of Science, Babylon University, Hillah, Iraq.
E-mail: o.al-owaedi@lancaster.ac.uk
[d] Dr. V M García-Suárez, Prof. J. Ferrer
Departamento de Física, Universidad de Oviedo and CINN (CSIC), ES-33007 Oviedo, Spain.

Θ These authors contributed equally to this work.
Supporting information for this article is available on the WWW under http://www.chemeurj.org/ or from the author.

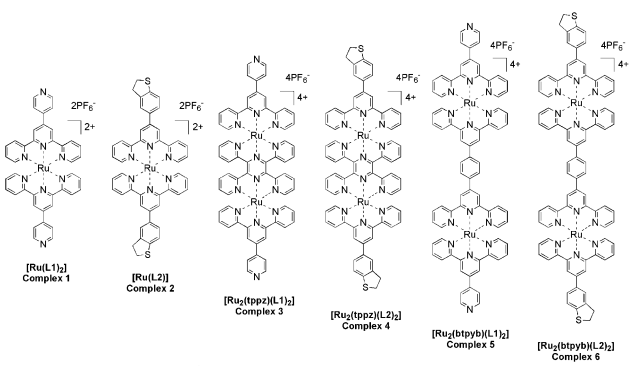

Figure 1. Structures of ruthenium complexes with pyridine (PY) and 2,3-dihydrobenzo [b] thiophene (BT) anchors and their numerical designation.

Their conductance properties can be tuned by electrochemical gating,[10] light irradiation[11] and by applying magnetic field.[12] It has already been demonstrated that introducing metal centers into the molecular backbone can lead to a significant improvement of the conductance.[13] Wang et al. showed that the incorporation of ferrocene into the OPE backbone leads to a significantly improved conductance in the tunneling and hopping regimes as compared to the conventional OPE molecules.[14] The electric conductance in the tunneling regime exponentially decreases as a function of molecular length according to $G=G_c e^{-\beta L}$, where β is tunneling decay parameter, G_C is the contact conductance and L refers to the molecular length, respectively. Sedghi et al. reported a very low attenuation factor of β = 0.004 nm^{-1} for a series of porphyrin-based molecular wires.[15] Li et al. observed similar results with meso-to-meso ethyne-bridged (porphinato)zinc(II) structures connected to gold electrodes via (4-thiophenyl)ethynyl termini, are determined using STM-BJ method (β = 0.0034 nm^{-1}).[16] Wen et al. showed that sulfur functionalized organometallic wires with ruthenium (II) centers have significantly higher conductance comparing to oligo(phenylene-ethylene) (OPE) but exhibit weaker length dependence.[17] Devidson et al reported the synthesis of a series of ruthenium complexes with different molecular lengths and functionalized with thiomethyl anchoring groups.[10c] STM-based single molecular conductance measurements showed the exponential decay of conductance as a function of molecular length with a decay parameter of 1.5 nm^{-1}.[18] The choice of the linker group determines the range of relative orientations of the molecule with respect to the electrode. From previous studies it is known that pyridine (PY), 2,3-dihydrobenzo [b] thiophene (BT) units serving as anchor groups provide a uniform distribution of conductances in the break junction experiment.[19] Although, there are some reports on the charge transport study of organometallic complexes (length dependence,[17-18] electrochemical gating[10b] and etc) to the best of our knowledge, the anchoring group effect on the charge transport properties of ruthenium complexes has not been studied systematically. Here, we report the synthesis, electrochemical and single molecule conductance measurement of a series of ruthenium complexes functionalized with pyridine (PY) and 2,3-dihydrobenzo [b] thiophene (BT) anchor groups. Fig. 1 shows the series of ruthenium complex molecules that we have used to study the particular influence of the molecular length and the chemical nature of the anchor group on the resulting transport properties. The transport properties of the complexes in Au/single complex/Au junctions were studied by means of the STM-BJ method. DFT-based calculations provide additional information on the electronic structure of those metal complexes in the single molecular junction. Most importantly, we aim to develop a fundamental understanding of the molecular length and anchoring group dependence of the electronic structure and charge transport properties of those ruthenium complexes that are confined in these single molecular junctions.

Results and Discussion

Synthesis

We synthesized six ruthenium complexes containing three different ruthenium cores with different anchor groups, pyridyl (PY) and 2,3-dihydrobenzo [b] thiophene (BT), as depicted in the supporting information in Schemes S1 and S2. Both PY and BT groups are known to be good anchoring groups for the gold substrate and STM tip.[19c] 4'-(4-pyridyl)-2,2':6',2''-terpyridine **L1** were synthesized by the previously reported route.[20] For ligand **L2**, the condensation reaction of 2-acetylpyridine with BT aldehyde occurred in similar to that previously described for terpyridine ligands .[20-21] Complex **1** and **2** were synthesized by the reaction of $[Ru(L)Cl_3]$ and ligand L at the ratio of 1:1 in ethylene glycol under microwave irradiation. For the preparation of the dinuclear complexes (complex **3-6**), the microwave-assisted substitution reaction of ancillary ligand (**L1** and **L2**) with dinuclear starting complex, ($[Cl_2(EtOH)Ru(tppz)RuCl_3]$ or $[Cl_2(EtOH)Ru(btpyb)RuCl_3]$ at a ratio of 2:1 afforded the product, where tppz and btpyb stand for 2,3,5,6-tetra(pyridine-2-yl)pyrazine and 1,4-bis(2,2':6',2''-terpyridin-4'-yl)benzene respectively.[22] These complexes were purified by Sephadex LH-20 gel-filtration chromatography and characterized by ^{1}H NMR and ESI-TOF-Mass.

Cyclic voltammogram

Figure 2 shows the electrochemical behaviour of the complexes studied by cyclic voltammetry (CV) and differential pulse voltammetry (DPV). Key electrochemical data derived for those CVs are summarized in Table 1. The CV of complex **1** shows a well-defined one-electron oxidation wave at 0.94 V vs Fc^+/Fc, which can be attributed to be metal-based (Ru^{II}/Ru^{III}) redox-reaction. In addition, two subsequent one-electron reduction waves at −1.53 and −1.77 V vs Fc^+/Fc correspond to the reductions of the ancillary ligands. Complex **2** exhibits one oxidation wave and three reduction waves at 0.89 (irr), -1.63 and -1.87 V vs Fc^+/Fc. The oxidation peak at 0.89 V was attributed to the superposition of the $Ru^{II/III}$ couple and the oxidation of **L2** ligand. From the separate cyclic voltammetric experiment of **L2** only, irreversible oxidation process was observed at E_{pa}= +0.61 V (irr) for the oxidation of dihydrobenzo [b] thiophene group together with two reduction peaks at -2.41 (E_{pc}, irr), and -2.81 V(E_{pc}, irr) for the reduction of terpyridine moiety (Figure S1). Therefore, the two reduction waves at -1.63 and -1.87 V vs Fc^+/Fc correspond to one-electron reductions of each peripheral ligand **L2** in the complex **2**. The large spike peak at E_{pc} =-1.71 V vs Fc^+/Fc might be associated to the desorption of the adsorbed reduced species.[23] Complex **3** exhibits well-defined two one-electron oxidation waves at 1.06 and 1.39 V vs Fc^+/Fc and two one-electron reduction waves at −0.74 and −1.23 V vs Fc^+/Fc. According to redox behaviour of similar dinuclear ruthenium complexes reported previously, the oxidation waves correspond to (Ru^{II}-Ru^{II})/ (Ru^{II}-Ru^{III}) and (Ru^{II}-Ru^{III})/ (Ru^{III}-Ru^{III}) processes, respectively.[18, 24] The reduction waves correspond to tppz/$tppz^-$ and $tppz^-$/$tppz^{2-}$ processes. In the more negative potential region, a reduction wave at -1.75 V vs Fc^+/Fc for the reduction of ancillary **L1** ligands was observed as a two-electron process, associated with a large desorption spike peak at -1.58 V during the reverse positive scanning. Complex **4** exhibits two oxidations at 1.03 V and 1.35 V vs Fc^+/Fc waves in addition to the oxidation of ancillary ligands at 0.94 V. Further, three reduction waves were observed at -0.76, -1.25, and -1.75 V Fc^+/Fc, each of which was assigned to the successive reductions of tppz and two- electron reductions of ancillary ligands. The small desorption peak was observed at -1.69 V vs Fc^+/Fc. In the case of the of complex **5**, a two-electron oxidation wave at 0.94 V vs $Fc^{+/}$Fc correspond to

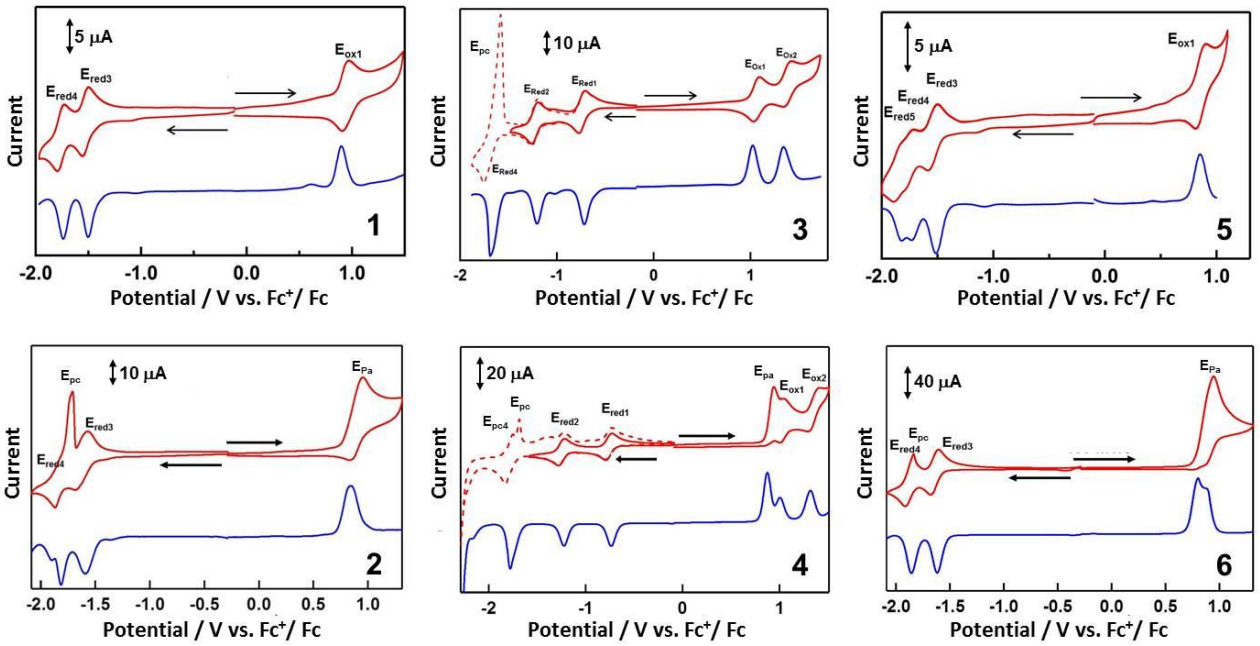

Figure 2. Cyclic voltammograms (red curves) and differential pulse voltammograms (blue curves) of complexes **1**-**6** in CH_3CN/0.1 M $TBAPF_6$ at room temperature. The number inside the graphs correspond to the complexes in Figure 1.

Table 1. Electrochemical data for complexes **1**-**6** in CH_3CN (0.1 M $TBAPF_6$) at room temperature

	$E_{1/2}$ / V vs. Fc^+ / Fc (ΔE_p/mV)							
	Reduction					Oxidaton		
complex	$E_{1/2\ Red5}$	$E_{1/2\ Red4}$	$E_{1/2\ Red3}$	$E_{1/2\ Red2}$ $tppz^{-/2-}$	$E_{1/2\ Red1}$ $tppz^{0/-}$	E_{pa}	$E_{1/2\ Ox1}$	$E_{1/2\ Ox2}$
1		-1.77(53)	-1.53(59)				0.94(52)	
2		-1.87[a]	-1.63(110)			0.89(irr)		
3		-1.75[a](2e)[b]		-1.23(57)	-0.74(64)		1.06(57)	1.39(85)
4		-1.79(70)[a](2e)[b]		-1.25(61)	-0.76(54)	0.94(irr)	1.03(44)	1.35(100)
5	-1.86 (72)	-1.75(60)	-1.54(72)				0.86(83)	
6		-1.92 [a]	-1.64(69)			0.94(irr)		

[a]Desorption spike observed in the reverse anodic scan. [b] two electron process was observed.

Ru(II/III) couple of isolated two ruthenium cores and three reduction peaks at -1.54 and -1.75 and -1.86 V vs Fc^+/Fc attributed to reductions of ancillary ligands and bridging ptpy. As with complex **5**, the cyclic voltammogram of complex **6** displays one oxidation and two reduction waves observed at 0.94, -1.64, and -1.92 V Fc^+/Fc. When **L2** was used as the peripheral ligand, not only Ru^{II}/Ru^{III} oxidation processes but also **L2** oxidation were involved in the redox events. The DPV of complexes **2**, **4**, and **6** can be confirmed that the oxidation process of **L2** peripheral ligand was involved (Figure 2).

Single molecular break-junction experiments:

The transport properties of single molecular ruthenium complex wires were studied using STM-BJ in solution (typically 20 μM solution of target molecules in tetrahydrofuran (THF) / 1,3,5-trimethyl benzene (TMB) 1:4 v/V), at room temperature and under argon atmosphere. The STM-BJ approach is based on the repeated formation and breaking of single molecule junctions between an atomically-sharp gold STM tip and a flat Au(111) substrate, and the simultaneous monitoring of the current i_T or conductance $G = i_T/V_{bias}$ at constant bias voltage typically at V_{bias} = 100 mV/s.[3a, 25] More detailed information on the instrumentation and experimental protocols can be found in the experimental section and in our previous publications.[19b, 25]

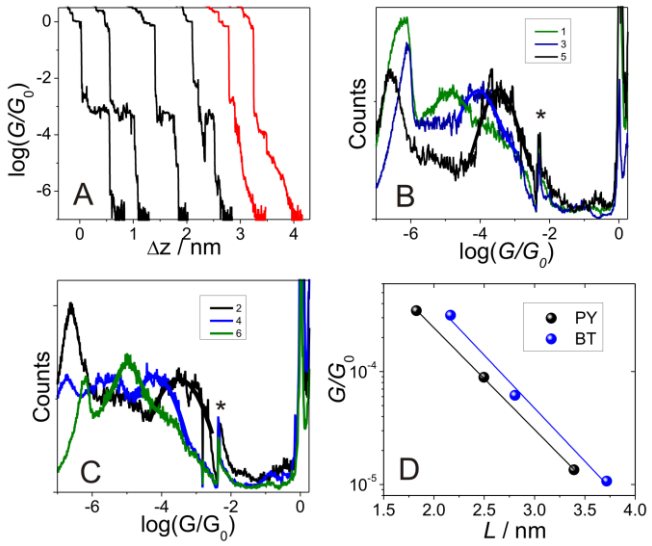

Figure 3 Conductance measurements of ruthenium complex molecular wires in TMB/THF (4 : 1, v/v) employing a STM-BJ recorded with V_{bias} = 0.1 V and a stretching rate of 58 nm s^{-1}. (A) typical conductance-distance traces of complex **1**, traces with molecule in the junction (black curves) and traces without molecule in the junction (red curves). (B,C) 1D conductance histograms of PY(**1**,**3**,**5**) and BT(**2**,**4**,**6**) terminated ruthenium complex molecular wires. ("*" The small spike at log(G/G_0) ≈ -2.3 in panel B,C is an artifact related to the switching of the amplifier stage.). (A) Most probable single junction conductance values of the two families of ruthenium complex molecular wires as determined from the analysis of 1D conductance histograms verses the molecular length (*L*).

Figure 3A displays typical conductance log(G/G_0) versus distance (Δz) traces from the measurements with pyridine terminated ruthenium complex **1**. All traces show initially a step like decrease of conductance from 10 G_0 to 1 G_0 at integer multiples of the quantum conductance $G_0 = 2e^2/h$ = 77.5 μS. Upon further stretching, the current abruptly decreases by several orders of magnitude and additional features, such as single conductance plateaus are observed at $G < G_0$, which are attributed to the formation of a single molecular junction. Due to the low concentration of the complex in solution, a very small number of the cycles demonstrated a successful formation of a junction (>20% of curves) whereas the remaining curves showed pure tunneling behavior (red curves in fig.3A). Figure 3(B,C) displays one dimensional (1D) histograms of ruthenium complexes with PY(**1**,**2**,**5**) and BT(**2**,**4**,**6**) anchoring groups plotted in logarithmic scale. We observed clear peaks for the breaking of Au–Au contacts as marked by integers of G_0, and one well-defined peak related to the molecular-junction. Most probable conductance values were obtained from Gaussian fits of the molecular junction peaks.

Figure 3D displays the most probable conductances of the ruthenium complexes (**1-6**) as function of their molecular length (*L*). The analysis of the most probable conductance values reveals an exponential dependence on the molecular length (L) with decay constants of β_{BT}= 2.07±0.1 and β_{Py} = 2.16±0.1. Decay constant values observed in this study are similar to the values eported by Davidson et al.,[18] for ruthenium complexes with thiomethyl anchoring groups (β_{SMe} = 1.5 nm^{-1}). These values are comparable to other π-conjugated molecular wires such as oligo(phenylene-ethynylenes) (OPEs, 2.0 - 3.4 nm^{-1}),[3b, 14, 26] oligophenyleimine (OPI, 3 nm^{-1}),[27] carotenoid polyenes (1.7 - 2.2 nm^{-1}),[28] oligo(phenylene-vinylenes) (OPVs, 1.7 - 1.8 nm^{-1}).[29] The small differences in decay constant values between PY anchoring and BT anchoring groups demonstrate that the nature

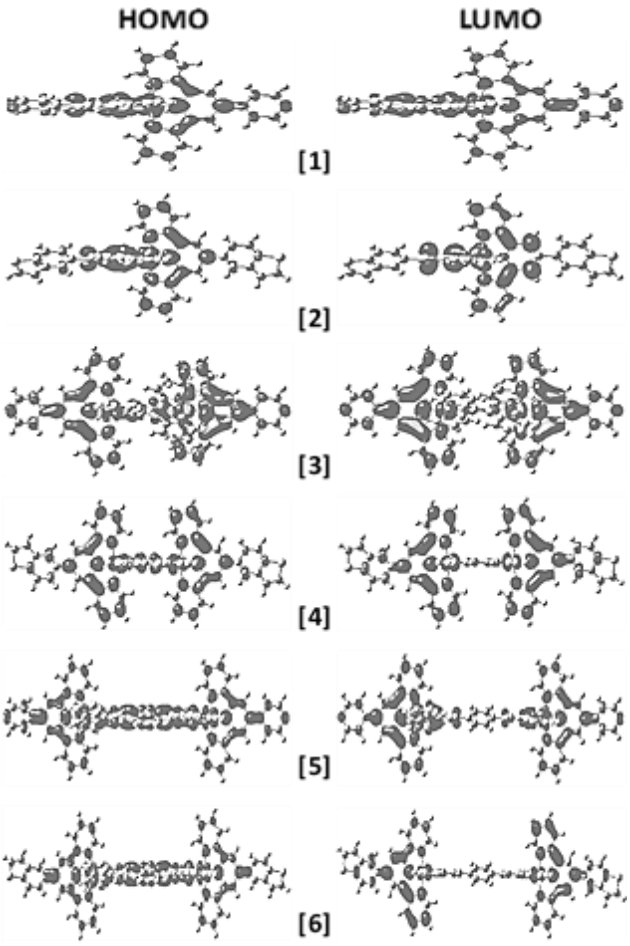

Figure 4. The iso-surfaces of the HOMOs and LUMOs for 1-6.

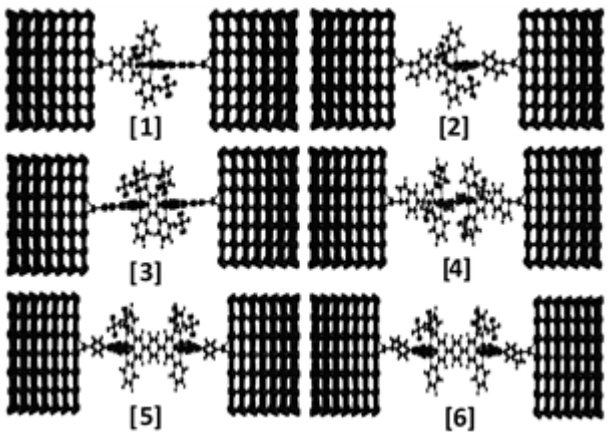

Figure 5. The relaxed structures of junctions 1-6.

of the anchor group controls the strength of the electronic coupling to the metal leads, the position of the energy levels involved in the electron transport across the single molecule junction as well as their coupling into the molecular wire backbone.[19c]

We also observed that the effective contact resistances $R_C = 1/G_C$, determined by extrapolating the G versus *L* dependencies towards L → 0), leads to the following sequence R_C(BT) < R_C(PY), which is consistent with the results reported for oligoyne

based molecular wires with BT and pyridine anchoring groups.[19c, 30]

Quantum Chemical Modelling

To further explore the electronic characteristics of these compounds and the electrical behavior of the junctions, we turned to DFT based methods. Before calculating the transport properties, the gas-phase electronic structures of **1**–**6** were investigated to explore the influence of ligands on the distribution and composition of the frontier molecular orbitals. The B3LYP level of theory[31] with LANL2DZ basis set[32] was used. Plots of the HOMOs and LUMOs are given in Figures 4 and S12.

The quantum chemical computations indicate that the HOMOs for complexes **3-6** are mainly localized on π-type conjugated pathway between the two Ru^{II} atoms, which is consistent with the direction of electron transport, as expected from previous studies.[17] In contrast, the LUMOs are distributed on orbitals of the ancillary

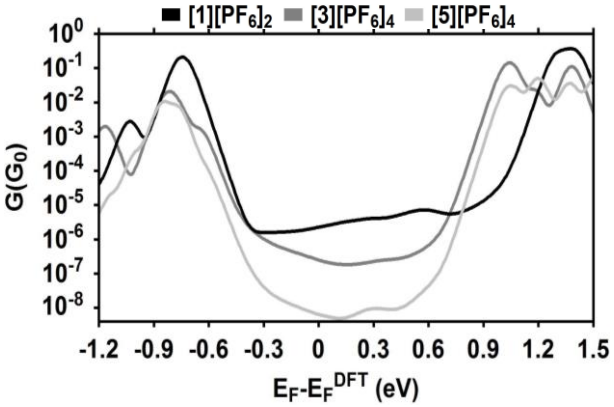

Figure 6. Plots of theoretically computed room temperature conductances of Au-PY-Au junctions as a function of the Fermi energy.

terpyridyl ligands on each side of the molecule. In this case the electronic density resident on the backbone between ruthenium atoms is ultra-short, which is unfavorable for electron transport. The HOMOs are more metal in character (42%), while the complexes offer LUMOs that are less metallic in character (33%).

To compute their transport properties we placed the optimised structures (molecule and counter ions) between gold electrodes (single-add atom electrodes) grown along the (111) direction; we used 7 layers of 49 atoms on each electrode plus single atom, making a total of 344 atoms per electrode. The molecules and counter ions together were allowed to relax to yield the structures shown in Figures 5, S10 and S11. To model the effect of an electrochemical environment, we used two hexafluorophosphate $[PF_6]^-$ counter ions for structures **1** and **2**, and four counter ions for structures **3**, **4**, **5** and **6**. In this study, simulations were carried out with 6 different optimal distances χ between the fluorine atoms of counter ions and nitrogen atoms of the backbone[18]; see supplementary information for all electrochemical computational details.

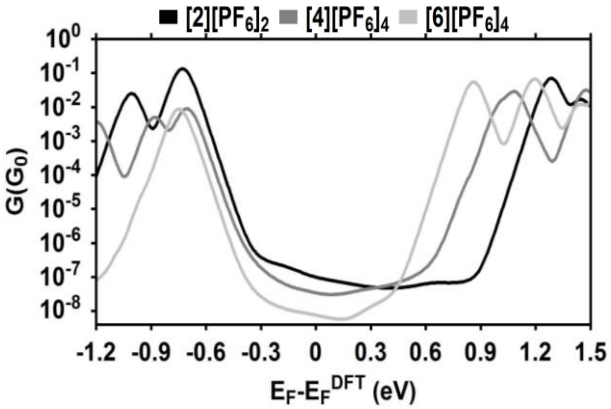

Figure 7. Plots of theoretically computed room temperature conductances of Au-BT-Au junctions as a function of the Fermi energy.

Table 2. The experimental ($G(G_0)_{Ex.}$) and theoretical ($G(G_0)_{Th.}$) conductances and decay constants (β) at E_F-E_F^{DFT}=-0.53 eV. The molecular length (L) is the optimal distance between sulfur-sulfur atoms for Au-BT-Au junctions and nitrogen-nitrogen atoms for Au-PY-Au junctions.

System	$G(G_0)_{Th.}$	$G(G_0)_{Ex.}$	L (nm)	$\beta_{Th.}$ (nm^{-1})	$\beta_{Ex.}$ (nm^{-1})
$[1][PF_6]_2$	3.55×10^{-4}	3.47×10^{-4}	1.825	2.05	2.07
$[3][PF_6]_4$	8.97×10^{-5}	8.91×10^{-5}	2.496		
$[5][PF_6]_4$	1.43×10^{-5}	1.35×10^{-5}	3.391		
$[2][PF_6]_2$	3.21×10^{-4}	3.16×10^{-4}	2.165	2.16	2.16
$[4][PF_6]_4$	6.31×10^{-5}	6.17×10^{-5}	2.805		
$[6][PF_6]_4$	1.09×10^{-5}	1.07×10^{-5}	3.717		

The calculated conductances as a function of the Fermi energy for Ru^{II} complexes for two model molecular junction systems including Au-BT-Au and Au-PY-Au models are shown in Figures 6 and 7. Although, a strong bond is formed between sulfur and gold atoms,[33] our results indicate that the conductance of the Au-PY-Au structures is higher than that of Au-BT-Au structures. This result is due to the alignment between the molecular orbitals and the gold Fermi level, since the Fermi level of gold electrodes lies

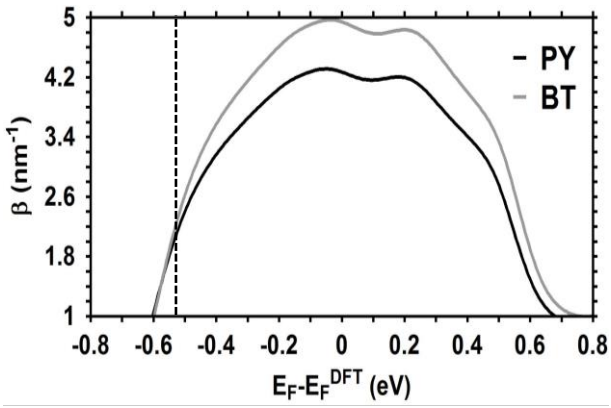

Figure 8. Conductance decay constant β (nm^{-1}) for the complex series 1-6 as a function of the Fermi energy. A black dashed line shows the choisen Fermi energy (E_F=-0.53 eV)

in between HOMO-LUMO gap. Thus, to enhance the contribution of the orbitals of Ru^{II} to the current, one should bring the HOMO level closer to the gold Fermi level, which is consistent with previous studies.[34] In addition, the conductance of the

complexes containing one Ru^{II} redox centre is noticeably higher than that of complexes containing two Ru^{II} redox centres. Computed conductance trends (Table 2 and Fig. 7,8 and 9) reflects the charge-transport mechanism of phase-coherent tunnelling[35]. Furthermore, the short molecular length decreases the tunnelling distance, which leads to high conductance and vice versa.

It is worth to mention that the DFT-predicted Fermi energy (E_F^{DFT}) is not usually reliable[1f]. Therefore, we treat the Fermi energy E_F as a free parameter which we determine by comparing the calculated conductances of all molecules with experimental values and chose a single common value of E_F which gave the closest overall agreement. This yields a corrected value of E_F-E_F^{DFT}=-0.53 eV. Examples of similar corrections can be found in the literature.[1f, 36] Our results show that the conductance of both types of molecular junctions decay exponentially in agreement with the experimental data as shown in Figure 8 and Table 2.

Figure 8 shows the Fermi energy dependence of the decay constant (β) for the complex series with PY and BT anchor groups respectively. The best agreement between experiment and theory is shown in Figure 9, and it is obtained at E_F = -0.53 eV. (see also Fig S9 of the SI) With this choice of E_F both computational data in figures 6, 7, 9 and experimental data in figure 3 show that the order of the conductance at the chosen Fermi energy is [1] > [2] > [3] > [4] > [5] > [6]. In addition, the computational β values in figure 8 and table 2 follow the trend $\beta_{BT} > \beta_{PY}$. Figures 6, 7 and 9 show that the conductance and attenuation factor are sensitive to the position of the Fermi energy within HOMO-LUMO gap.

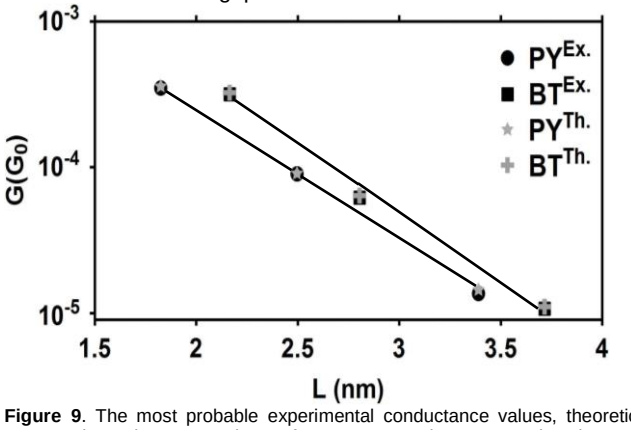

Figure 9. The most probable experimental conductance values, theoretically computed conductance values of Au-PY-Au and Au-BT-Au junctions as a function of molecular length (*L*). The theoretical conductance values are obtained at E_F-E_F^{DFT}=-0.53 eV.

Conclusion

We presented the synthesis, electrochemical and single molecule conductance characterization of two series of ruthenium complex molecular wires with pyridine (PY) and 2,3-dihydrobenzo [b] thiophene (BT) anchor groups. Cyclic voltammetry data showed clear redox peaks corresponding to both the metal and ligand redox reactions. Single molecular conductance results showed an exponential decay of the conductance with molecular length (decay constants of β_{BT}= 2.07±0.1 nm^{-1} and β_{PY} = 2.16 ±0.1 nm^{-1}), indicating the tunnelling mechanism. The small differences in decay constant values between PY anchoring and BT anchoring groups demonstrate that the nature of the anchor group controls the strength of the electronic coupling to the metal leads, the position of the energy levels involved in the electron transport across the single molecule junction as well as their coupling into the molecular wire backbone. We also observed that the effective contact resistances $R_C = 1/G_C$, determined by extrapolating the G versus L dependencies towards $L \rightarrow 0$), leads to the following sequence R_C(BT) < R_C(PY), which is consistent with the results reported for oligoyne based molecular wires with 2,3-dihydrobenzo [b] thiophene (BT) and pyridine (PY) anchoring groups. Density functional theory (DFT)-based calculations provided additional information on the electronic structure and charge transport properties in metal/ruthenium complex/metal junctions. A striking feature of the present calculations is that they point to HOMO-dominated transport, rather than the LUMO-dominated transport found in ref[10c], in which a series of bis-2,2:6,2-terpyridine complexes featuring Ru(II), Fe(II), and Co(II) metal ions was contacted to gold electrodes using trimethylsilylethynyl or thiomethyl surface anchor groups. This suggests that the anchor groups play a crucial role in fixing the position of the frontier orbitals relative to the Fermi energy; a prediction which could be tested by measuring the sign of their Seebeck coefficients.

Experimental Section

Synthesis: 4'-(4-pyridyl)-2,2':6',2''-terpyridine (ptpy, **L1**) and 5-bromo-2,3-dihydrobenzo[b]thiophene were synthesized according to previous reports. [19a, 20]

2,3-dihydrobenzo[b]thiophene-5-carboxaldehyde: Under argon atmosphere, to a solution of 5-bromo-2,3-dihydrobenzo[b]thiophene (1 g, 4.65 mmol), in dry THF (10 mL) cooled in a dry-ice-acetone bath was added dropwise n-butyllithium solution (1.6 M in hexane) (4 mL, 6.4 mmol). The solution was stirred for 1 h at low temperature followed by the addition of dry DMF (1.2 m, 15.5 mmol). The mixture was stirred for overnight while the temperature was allowed to rise to room temperature. 300 ml of CH_2Cl_2 was added to the reaction solution and the mixture was washed with water twice. The organic layer was dried over Na_2SO_4 and the solvent removed under reduced pressure. The crude product was purified by silica-gel column chromatography (CH_2Cl_2) to give a white solid (661 mg, 87%). ^{1}H NMR (500 MHz, $CDCl_3$) δ = 9.88 (s, 1H), 7.68 (s, 1H), 7.61 (d, *J* = 8 Hz, 1H), 7.34 (d, *J* = 8 Hz, 1H), 3.44 (t, *J* = 8 Hz, 2H), 3.36 (t, *J* = 8 Hz, 2H).

4'-(2,3-dihydrobenzo [b] thiophene)-2,2'-6',2"-terpyridine L2 (bttpy**, L2**): 2,3-dihydrobenzo[b]thiophene-5-carboxaldehyde (661 mg, 4.03 mmol), 2-acetylpyridine (1ml, 8.93 mmol), solid NaOH (400 mg, 10 mmol), and 30% NH_3aq (4ml) were mixed and stirred at 100 °C for 17 h. The reaction solution was cooled to room temperature. 300 ml of water was added the solution and the precipitation was filtrated. The filtrate was washed with methanol several times to give white solid (707 mg, 48%). ^{1}H NMR (500 MHz, $CDCl_3$) δ = 8.65-8.75 (m, 6H), 7.88 (t, *J* = 7.7 Hz, 2H), 7.77 (s, 1H), 7.31-7.38 (m, 3H), 3.36-3.47 (m, 4H).

Complex 1: [Ru(ptpy)Cl_3] (50 mg, 0.097 mmol) and 4'-(4-pyridyl)-2,2':6',2''-terpyridine (ptpy) (30 mg, 0.097 mmol) was added in 5 ml of ethylene glycol and the mixture solution was refluxed for 5 min under microwave irradiation (Sikoku Keisoku Ltd. 650 W multimode). When the solution was turned to reddish brown, the solution was cooled to room temperature. 20 ml of water and saturated KPF_6aq was added to the solution, which affected the precipitation of the solid product. The precipitate was purified by Sephadex LH-20 (eluent: 1:1, CH_3CN/CH_3OH, second band) to give [Ru(ptpy)$_2$](PF_6)$_2$ (20.6 mg, 21%). ^{1}H NMR ($CDCN_3$) δ = 9.05 (s, 4H), 8.96 (d, 4H, J = 4 Hz), 8.65 (d, 4H, J = 8 Hz), 8.13 (d, 4H, J = 4 Hz), 7.96 (t, 4H, J = 8 Hz), 7.41 (d, 4H, J = 6 Hz), 7.19 (t, 4H,

J = 6 Hz). ESI-TOF MS m/z: 361.07 calcd for $[M - 2PF_6]^{2+}$, found 361.06.

Complex 2: To 5 ml of ehtyele glycol was added $[Ru(bttpy)Cl_3]$ (107 mg, 0.186 mmol) and 4'-(2,3-dihydrobenzo [b] thiophene)-2,2'-6',2"-terpyridine (bttpy) (68 mg, 0.185 mmol). The mixture was heated microwave irradiation for 6 min (650 W). After the solution was cooled to room temperature, 20 ml of water and saturated KPF_6aq was added to the solution. After being filtered, the obtained solid was purified by Sephadex LH-20 (eluent: 1:1, CH_3CN/CH_3OH, second band). Removal of the solvent in vacuo yielded the product as a purple solid. (88 mg, 42%). ^{1}H NMR ($CDCN_3$) δ = 8.96 (s, 4H), 8.62 (d, 4H, J = 8 Hz), 8.08 (s, 2H), 7.93 (m, 6H), 7.57 (d, 2H, J = 8 Hz), 7.41 (d, 4H, J = 5 Hz), 7.16 (t, 4H, J = 6 Hz) 3.53 (m, 8H). ESI-TOF MS m/z: 417.06 calcd for $[M - 2PF_6]^{2+}$, found 417.29.

Complex 3: $[Cl_3Ru(tppz)RuCl_2(EtOH)]$ (49.8 mg, 0.0612 mmol) and ptpy (42.1 mg, 0.136 mmol) was added in 5 ml of ethylene glycol. The mixture solution was refluxed for 4 min by 650 W of microwave irradiation, which induced a rapid color change to green. After being cooled to room temperature, the reaction solution was diluted with 20 ml of water. After addition of saturated KPF_6aq, the resulting precipitate was collected by filtration. The residue was washed with water and purified by Sephadex LH-20 column chromatography using CH_3CN/CH_3OH (1:1 v/v, third band) as eluent, yielded $[Ru_2(tppz)(ptpy)_2](PF_6)_4$ as purple solid. (50.0 mg, 45%). ^{1}H NMR ($CDCN_3$) δ = 9.20 (s, 4H), 9.06 (d, 4H, J = 4 Hz), 8.97 (d, 4H, J = 8 Hz), 8.79 (d, 4H, J = 8 Hz), 8.24 (d, 4H, J = 6 Hz), 8.10 (t, 4H, J = 8 Hz), 7.93 (t, 4H, J = 8 Hz), 7.79 (m, 8H), 7.43 (d, 4H, J = 6 Hz), 7.33 (t, 4H, J = 6 Hz). ESI-TOF MS m/z: 303.05 calcd for $[M - 4PF_6]^{4+}$, found 303.04.

Complex 4: bttpy (49.6 mg, 0.135 mmol) and $[Cl_3Ru(tppz)RuCl_2(EtOH)]$ (50.0 mg, 0.0614 mmol) were added in 5 ml of ethylene glycol and the mixture solution was heated for 4 min under microwave irradiation (650 W). The reaction mixture was then cooled to room temperature and 20 ml of water was added, and the precipitate was obtained by addition of an excess KPF_6. The resulting precipitate was subjected to gel filtration chromatography on Sephadex LH-20 (eluent: 1:1, CH_3CN/CH_3OH, third band), affording $[Ru_2(tppz)(ptpy)_2](PF_6)_4$ as purple solid. (89.2 mg, 76%). ^{1}H NMR ($CDCN_3$) δ = 9.11 (s, 4H), 8.96 (d, 4H, J = 8 Hz), 8.75 (d, 4H, J = 8 Hz), 8.16 (s, 2H), 8.07 (m, 6H), 7.93 (t, 4H, J = 9 Hz), 7.82 (d, 4H, J = 6 Hz), 7.72 (d, 4H, J = 6 Hz), 7.64 (d, 2H, J = 8 Hz), 7.42 (t, 4H, J = 7 Hz), 7.29 (t, 4H, J = 7 Hz), 3.58 (m, 8H). ESI-TOF MS m/z: 331.45 calcd for $[M - 4PF_6]^{4+}$, found 331.64.

Complex 5: $[Ru(ptpy)Cl_3]$ (50 mg, 0.0966 mmol) and 1,4-di(2,2':6',2''-terpyridine-4'-yl)benzene (btpyb) (26.1 mg, 0.0483 mmol) were dissolved in 4 ml of ethylene glycol. The mixture solution was refluxed by microwave irradiation for 6 min (650 W). During heating, the solution color was changed from red brown to brown. After the solution was cooled to room temperature, 20 ml of water and an excess of KPF_6 was added the solution. The resulting precipitate was collected by filtration. The $[Ru_2(btpyb)(ptpy)_2](PF_6)_4$ was purified by Sephadex LH-20 (eluent: 1:1, CH_3CN/CH_3OH, third band) and isolated by evaporation of the solvent and dried in vacuo. (12.2 mg, 13%). ^{1}H NMR ($CDCN_3$) δ = 9.27 (s, 4H), 9.11 (s, 4H), 8.98 (d, 4H, J = 6 Hz), 8.84 (d, 4H, J = 8 Hz), 8.72 (d, 4H, J = 8 Hz), 8.66 (s, 4H), 8.18 (d, 4H, J = 6 Hz), 8.00 (m, 8H), 7.52 (d, 4H, J = 5 Hz), 7.46 (d, 4H, J = 5 Hz), 7.24 (m, 8H). ESI-TOF MS m/z: 341.06 calcd for $[M - 4PF_6]^{4+}$, found 341.03.

Complex 6: To 20 ml of acetone was added $[Cl_3Ru(btpyb)RuCl_2(CH_3CH_2OH)]$ (100 mg, 0.10 mmol) and CF_3SO_3Ag (150 mg, 0.58 mmol) and the mixture solution was refluxed for 3 h under dark condition. The solution was filtrated by celite to remove the insoluble solid and the solvent was evaporated. 4'-(2,3-Dihydrobenzo [b] thiophene)-2,2'-6',2"-terpyridine (bttpy) 100 mg (0.27 mmol) and 10 ml of ethylene glycol were added and the mixture solution was refluxed at 200 °C for 3h. After being cooled to room temperature, 20 ml of water and saturated KPF_6aq was added the solution and the precipitate was filtrated. The obtained solid was purified by silica gel chromatography using acetone/ saturatedKNO_3aq (9/1 v/v) and Sephadex LH-20 using CH_3CN/CH_3OH (1/1 v/v, third) as eluent to give $[Ru_2(btb)(bttpy)_2](PF_6)_4$ (37 mg, 18%). ^{1}H NMR ($CDCN_3$) δ = 9.17 (s, 4H), 9.11 (s, 4H), 8.74 (d, 4H, J = 8 Hz), 8.66 (d, 4H, J = 8 Hz), 8.58 (s, 4H), 8.10 (s, 2H), 7.98 (m, 10H), 7.59 (d, 2H, J = 8 Hz), 7.47 (m, 8H), 7.21 (m, 8H), 3.55 (m, 8H). ESI-TOF MS m/z: 369.56 calcd for $[M - 4PF_6]^{4+}$, found 369.75.

Electrochemical Measurements

All cyclic voltammetry (CV) measurements were taken using a ALS model 660A potentiostat with a one compartment electrochemical cell under an atmosphere of argon. A glassy-carbon electrode with a diameter of 0.3 mm was used as the working electrode. The electrode was polished prior to use with 0.05 µm alumina and rinsed thoroughly with water and acetone. A large area platinum-wire coil was used as the counter electrode. All potentials were measured on a saturated $Ag/AgNO_3$ (0.01 M $AgNO_3$ in 0.1 M $TBAPF_6$ in CH_3CN) electrode as a reference and converted to a ferrocenium/ferrocene (Fc^+/Fc) couple without regard for the liquid junction potential. All measurements were carried out in acetonitrile with 0.1 M $TBAPF_6$ as the supporting electrolyte.

Single molecule conductance measurements

The STM-BJ measurements were carried out with a Molecular Imaging PicoSPM housed in an all-glass argon-filled chamber and equipped with a dual preamplifier capable of recording currents in a wide range of 1 pA to 150 µA with high resolution. The sample electrodes were Au (111) disks, 2 mm height and 10 mm in diameter, or gold single crystal bead electrodes. The Au (111) substrates were flame-annealed prior to use. A freshly prepared solution containing typically 20 µM of the molecule was added to a Kel-F flow-through liquid cell mounted on top of the sample. The STM tips were prepared by, electrochemical etching of the gold wires (Goodfellow, 99.999 %, 0.25 mm diameter). For each molecule up to 3000 traces were recorded for each set of experimental conditions to guarantee the statistical significance of the results. For further technical details and data analysis procedures we refer to our previous work.[3b, 19b]

Theoretical Section

Geometrical optimizations were carried out using the DFT code SIESTA, with a generalized gradient approximation (PBE functional),[37] double-zeta polarized basis set, 0.01 eV/A force

tolerance and a real-space grid with a plane wave cut-off energy of 250 Ry, zero bias voltage and 1 k points. To compute the electrical conductance of the molecules, they were each placed between gold electrodes. The complex cations and their associated counter ions were then placed in the vicinity of the metal | molecule | metal junctions. The complexes and counter ions were again allowed to relax, to yield the structures shown in Figure 5. For each structure, the transmission coefficient *T(E)* describing the propagation of electrons of energy E from the left to the right electrode was calculated by first obtaining the corresponding Hamiltonian and overlap matrices using SIESTA and then using the GOLLUM code[38] to compute *T(E)* via the relation $\mathrm{T(E)} = \mathrm{Tr}\{\Gamma_R(E)G^R(E)\Gamma_L(E)G^{R\dagger}(E)\}$, in this expression, $\Gamma_{L,R}(E) = i\left(\sum_{L,R}(E) - \sum_{L,R}{}^{\dagger}(E)\right)$ describes the level broadening due to the coupling between left (L) and right (R) electrodes and the central scattering region, $\sum_{L,R}(E)$ are the retarded self-energies associated with this coupling and $G^R = (ES - H - \sum_L - \sum_R)^{-1}$ is the retarded Green's function, where H is the Hamiltonian and S is the overlap matrix (both of them obtained from SIESTA). Finally the room temperature electrical conductance G was computed from the formula $G = G_0 \int_{-\infty}^{\infty} dE\, T(E)(-\frac{df(E)}{dE})$ where $f(E) = [e^{\beta(E-E_F)} + 1]^{-1}$ is the Fermi function, $\beta = 1/k_BT$, E_F is the Fermi energy and $G_0 = \left(\frac{2e^2}{h}\right)$ is the quantum of conductance. Since the quantity $(-\frac{df(E)}{dE})$ is a probability distribution peaked at $E=E_F$, with a width of the order k_BT, the above expression shows that G/G_0 is obtained by averaging T(E) over an energy range of order k_BT in the vicinity of $E=E_F$. It is well-known that the Fermi energy E_F^{DFT} predicted by DFT is not usually reliable and therefore we shown plots of $G(G_0)$ as a function of $E_F - E_F^{DFT}$. To determine E_F, we compared the predicted values of all molecules with the experimental values and chose a single common value of E_F which gave the closest overall agreement.[1f,39] This yielded a value of $E_F - E_F^{DFT} = -0.53$ eV, which is used in all theoretical results.

Acknowledgements

We acknowledge the financial support from the Swiss National Science Foundation (Grant No. 200020-144471); SCCER Heat and Electricity storage; M. H. acknowledges the financial support from the Institute of Science and Engineering at Chuo University. H. O. is grateful to "Tokuyama Science Foundation. C. J. L. and O. A. A. acknowledge financial support from the Ministry of Higher Education and Scientific Research of Iraq. V. M. G.-S. and J. F. thank the Spanish MICINN for funding (Grant No. FIS2012-34858). V. M. G.-S. also thanks the Spanish MICINN for a Ramón y Cajal Fellowship (RYC-2010-06053).

Keywords: Ruthenium complex • Molecular wire • STM-Break junction • Anchoring group • Electrochemistry

References

[1] a) R. L. McCreery, H. Yan and A. J. Bergren, *Physical Chemistry Chemical Physics* **2013**, *15*, 1065-1081; b) C. Joachim and M. A. Ratner, *Proceedings of the National Academy of Sciences of the United States of America* **2005**, *102*, 8801-8808; c) N. J. Tao, *Nat Nano* **2006**, *1*, 173-181; d) S. V. Aradhya and L. Venkataraman, *Nat Nano* **2013**, *8*, 399-410; e) C. Jia and X. Guo, *Chemical Society Reviews* **2013**, *42*, 5642-5660; f) C. J. Lambert, *Chemical Society Reviews* **2015**, *44*, 875-888.

[2] a) H. B. Akkerman and B. de Boer, *Journal Of Physics-condensed Matter* **2008**, *20*, 013001; b) F. Schwarz and E. Loertscher, *Journal of Physics-Condensed Matter* **2014**, *26*.

[3] a) B. Xu and N. J. Tao, *Science* **2003**, *301*, 1221-1223; b) V. Kaliginedi, P. Moreno-Garcia, H. Valkenier, W. Hong, V. M. Garcia-Suarez, P. Buiter, J. L. H. Otten, J. C. Hummelen, C. J. Lambert and T. Wandlowski, *Journal of the American Chemical Society* **2012**, *134*, 5262-5275.

[4] a) B. Xu, X. Xiao and N. J. Tao, *Journal of the American Chemical Society* **2003**, *125*, 16164-16165; b) I. V. Pobelov, G. Meszaros, K. Yoshida, A. Mishchenko, M. Gulcur, M. R. Bryce and T. Wandlowski, *Journal of Physics-Condensed Matter* **2012**, *24*; c) M. F. M. Frei, S. V. Aradhya, M. Koentopp, M. S. Hybertsen and L. Venkataraman, *Nano Letters* **2011**, *11*, 1518-1523.

[5] a) W. Hong, H. Valkenier, G. Meszaros, D. Z. Manrique, A. Mishchenko, A. Putz, P. M. Garcia, C. J. Lambert, J. C. Hummelen and T. Wandlowski, *Beilstein Journal of Nanotechnology* **2011**, *2*, 699-713; b) A. I. Yanson, G. R. Bollinger, H. E. van den Brom, N. Agrait and J. M. van Ruitenbeek, *Nature* **1998**, *395*, 783-785.

[6] A. S. Blum, J. G. Kushmerick, D. P. Long, C. H. Patterson, J. C. Yang, J. C. Henderson, Y. X. Yao, J. M. Tour, R. Shashidhar and B. R. Ratna, *Nature Materials* **2005**, *4*, 167-172.

[7] a) R. C. Chiechi, E. A. Weiss, M. D. Dickey and G. M. Whitesides, *Angewandte Chemie-International Edition* **2008**, *47*, 142-144; b) C. A. Nijhuis, W. F. Reus and G. M. Whitesides, *Journal of the American Chemical Society* **2009**, *131*, 17814-17827.

[8] N. Tuccitto, V. Ferri, M. Cavazzini, S. Quici, G. Zhavnerko, A. Licciardello and M. A. Rampi, *Nature Materials* **2009**, *8*, 41-46.

[9] a) H. Song, M. A. Reed and T. Lee, *Advanced Materials (Weinheim, Germany)* **2011**, *23*, 1583-1608; b) J. R. Heath, *Annual Review Of Materials Research* **2009**, *39*, 1-23; c) L. Sun, Y. A. Diaz-Fernandez, T. A. Gschneidtner, F. Westerlund, S. Lara-Avila and K. Moth-Poulsen, *Chemical Society Reviews* **2014**, *43*, 7378-7411.

[10] a) C. Li, A. Mishchenko, I. Pobelov and T. Wandlowski, *Chimia* **2010**, *64*, 383-390; b) T. Albrecht, K. Moth-Poulsen, J. B. Christensen, A. Guckian, T. Bjornholm, J. G. Vos and J. Ulstrup, *Faraday Discussions* **2006**, *131*, 265-279; c) Ross, Davidson, Oday A. Al-Owaedi, David C. Milan, Qiang Zeng, Joanne Tory, František Hartl, Simon J. Higgins, Richard J. Nichols, Colin J. Lambert, Paul J. Low. Inorg. Chem. articles ASAP DOI 10.1021/acsinorgchem.5b02094.

[11] F. Meng, Y.-M. Hervault, Q. Shao, B. Hu, L. Norel, S. Rigaut and X. Chen, *Nature Communications* **2014**, *5*.

[12] E. A. Osorio, K. Moth-Poulsen, H. S. J. van der Zant, J. Paaske, P. Hedegard, K. Flensberg, J. Bendix and T. Bjornholm, *Nano Letters* **2010**, *10*, 105-110.

[13] a) Z.-F. Liu, S. Wei, H. Yoon, O. Adak, I. Ponce, Y. Jiang, W.-D. Jang, L. M. Campos, L. Venkataraman and J. B. Neaton, *Nano Letters* **2014**, *14*, 5365-5370; b) A. C. Aragones, N. Darwish, W. J. Saletra, L. Perez-Garcia, F. Sanz, J. Puigmarti-Luis, D. B. Amabilino and I. Diez-Perez, *Nano Letters* **2014**, *14*, 4751-4756; c) F. Schwarz, G. Kastlunger, F. Lissel, H. Riel, K. Venkatesan, H. Berke, R. Stadler and E. Loertscher, *Nano Letters* **2014**, *14*, 5932-5940; d) F. Lissel, F. Schwarz, O. Blacque, H. Riel, E. Loertscher, K. Venkatesan and H. Berke, *Journal of the American Chemical Society* **2014**, *136*, 14560-14569; e) H. Masai, J. Terao, S. Seki, S. Nakashima, M. Kiguchi, K. Okoshi, T. Fujihara and Y. Tsuji, *Journal of the American Chemical Society* **2014**, *136*, 1742-1745.

[14] Q. Lu, C. Yao, X. Wang and F. Wang, *Journal of Physical Chemistry C* **2012**, *116*, 17853-17861.

[15] G. Sedghi, V. M. Garcia-Suarez, L. J. Esdaile, H. L. Anderson, C. J. Lambert, S. Martin, D. Bethell, S. J. Higgins, M. Elliott, N. Bennett, J. E. Macdonald and R. J. Nichols, *Nature Nanotechnology* **2011**, *6*, 517-523.

[16] Z. Li, T.-H. Park, J. Rawson, M. J. Therien and E. Borguet, *Nano Letters* **2012**, *12*, 2722-2727.

[17] H.-M. Wen, Y. Yang, X.-S. Zhou, J.-Y. Liu, D.-B. Zhang, Z.-B. Chen, J.-Y. Wang, Z.-N. Chen and Z.-Q. Tian, *Chemical Science* **2013**, *4*, 2471-2477.

[18] R. Davidson, J. H. Liang, D. C. Milan, B. W. Mao, R. J. Nichols, S. J. Higgins, D. S. Yufit, A. Beeby and P. J. Low, *Inorganic Chemistry* **2015**, *54*, 5487-5494.

[19] a) P. Moreno-Garcia, M. Gulcur, D. Z. Manrique, T. Pope, W. J. Hong, V. Kaliginedi, C. C. Huang, A. S. Batsanov, M. R. Bryce, C. Lambert and T. Wandlowski, *Journal of the American Chemical Society* **2013**, *135*, 12228-12240; b) W. Hong, D. Z. Manrique, P. Moreno-Garcia, M. Gulcur, A. Mishchenko, C. J. Lambert, M. R. Bryce and T. Wandlowski, *Journal of the American Chemical Society* **2012**, *134*, 2292-2304; c) V. Kaliginedi, A. V. Rudnev, P. Moreno-Garcia, M. Baghernejad, C. Huang, W. Hong and T. Wandlowski, *Physical Chemistry Chemical Physics* **2014**, *16*, 23529-23539.

[20] D. Q. Feng, X. P. Zhou, J. Zheng, G. H. Chen, X. C. Huang and D. Li, *Dalton Transactions* **2012**, *41*, 4255-4261.

[21] G. W. V. Cave and C. L. Raston, Journal of the Chemical Society-Perkin Transactions 1 **2001**, 3258-3264.

[22] R. C. Rocha, F. N. Rein, H. Jude, A. P. Shreve, J. J. Concepcion and T. J. Meyer, *Angewandte Chemie-International Edition* **2008**, *47*, 503-506.

[23] T. Nagashima, T. Nakabayashi, T. Suzuki, K. Kanaizuka, H. Ozawa, Y. W. Zhong, S. Masaoka, K. Sakai and M. Haga, *Organometallics* **2014**, *33*, 4893-4904.

[24] C. R. Arana and H. D. Abruna, *Inorganic Chemistry* **1993**, *32*, 194-203.

[25] V. Kaliginedi, P. Moreno-García, H. Valkenier, W. Hong, V. M. García-Suárez, P. Buiter, J. L. H. Otten, J. C. Hummelen, C. J. Lambert and T. Wandlowski, *Journal of the American Chemical Society* **2012**, *134*, 5262-5275.

[26] a) X. Zhao, C. Huang, M. Gulcur, A. S. Batsanov, M. Baghernejad, W. Hong, M. R. Bryce and T. Wandlowski, *Chemistry of Materials* **2013**, *25*, 4340-4347; b) Y. Xing, T.-H. Park, R. Venkatramani, S. Keinan, D. N. Beratan, M. J. Therien and E. Borguet, *Journal of the American Chemical Society* **2010**, *132*, 7946-7956; c) K. Liu, G. Li, X. Wang and F. Wang, *Journal of Physical Chemistry C* **2008**, *112*, 4342-4349.

[27] S. H. Choi, B. Kim and C. D. Frisbie, *Science* **2008**, *320*, 1482-1486.

[28] a) I. Visoly-Fisher, K. Daie, Y. Terazono, C. Herrero, F. Fungo, L. Otero, E. Durantini, J. J. Silber, L. Sereno, D. Gust, T. A. Moore, A. L. Moore and S. M. Lindsay, *Proceedings of the National Academy of Sciences of the United States of America* **2006**, *103*, 8686-8690; b) J. He, F. Chen, J. Li, O. F. Sankey, Y. Terazono, C. Herrero, D. Gust, T. A. Moore, A. L. Moore and S. M. Lindsay, *Journal of the American Chemical Society* **2005**, *127*, 1384-1385.

[29] a) I. W. P. Chen, M.-D. Fu, W.-H. Tseng, C.-h. Chen, C.-M. Chou and T.-Y. Luh, *Chemical Communications* **2007**, 3074; b) H. M. Liu, N. Wang, J. W. Zhao, Y. Guo, X. Yin, F. Y. C. Boey and H. Zhang, *Chemphyschem* **2008**, *9*, 1416-1424.

[30] a) M. Gulcur, P. Moreno-Garcia, X. Zhao, M. Baghernejad, A. S. Batsanov, W. Hong, M. R. Bryce and T. Wandlowski, *Chemistry-a European Journal* **2014**, *20*, 4653-4660; b) P. Moreno-Garcia, M. Gulcur, D. Z. Manrique, T. Pope, W. Hong, V. Kaliginedi, C. Huang, A. S. Batsanov, M. R. Bryce, C. Lambert and T. Wandlowski, *Journal of the American Chemical Society* **2013**, *135*, 12228-12240.

[31] a) A. D. Becke, *Journal of Chemical Physics* **1993**, *98*, 5648-5652; b) P. J. Stephens, F. J. Devlin, C. F. Chabalowski and M. J. Frisch, *Journal of Physical Chemistry* **1994**, *98*, 11623-11627.

[32] a) W. R. Wadt and P. J. Hay, *J. Chem. Phys.* **1985**, *82*, 284-298; b) P. J. Hay and W. R. Wadt, *Journal of Chemical Physics* **1985**, *82*, 270-283; c) P. J. Hay and W. R. Wadt, *Journal of Chemical Physics* **1985**, *82*, 299-310.

[33] J. M. Tour, *Accounts of Chemical Research* **2000**, *33*, 791-804.

[34] J. Ponce, C. R. Arroyo, S. Tatay, R. Frisenda, P. Gavina, D. Aravena, E. Ruiz, H. S. J. van der Zant and E. Coronado, *Journal of the American Chemical Society* **2014**, *136*, 8314-8322.

[35] B. Kim, J. M. Beebe, C. Olivier, S. Rigaut, D. Touchard, J. G. Kushmerick, X. Y. Zhu and C. D. Frisbie, *Journal of Physical Chemistry C* **2007**, *111*, 7521-7526.

[36] D. Z. Manrique, C. Huang, M. Baghernejad, X. Zhao, O. A. Al-Owaedi, H. Sadeghi, V. Kaliginedi, W. Hong, M. Gulcur, T. Wandlowski, M. R. Bryce and C. J. Lambert, *Nature Communications* **2015**, *6*, 6389.

[37] J. P. Perdew, K. Burke and M. Ernzerhof, *Phys. Rev. Lett.* **1996**, *77*, 3865-3868.

[38] J. Ferrer, C. J. Lambert, V. M. Garcia-Suarez, D. Z. Manrique, D. Visontai, L. Oroszlany, R. Rodriguez-Ferradas, I. Grace, S. W. D. Bailey, K. Gillemot, H. Sadeghi and L. A. Algharagholy, *New Journal of Physics* **2014**, *16*.

[39] Milan, David C., Al-Owaedi, Oday A., Oerthel, Marie-Christine, Marques-Gonzalez, Santiago, Brooke, Richard J., Bryce, Martin R., Cea, Pilar, Ferrer, Jaime, Higgins, Simon J., Lambert, Colin J., Low, Paul J., Manrique, David Zsolt, Martin, Santiago, Nichols, Richard J., Schwarzacher, Walther, Garcia-Suarez, Victor M. J. Phys. Chem. C, Article ASAP DOI: 10.1021/acs.jpcc.5b08877.

Received: ((will be filled in by the editorial staff))
Revised: ((will be filled in by the editorial staff))
Published online: ((will be filled in by the editorial staff))

DOI: 10.1002/chem.201xxxxxx

Table of Contents

FULL PAPER

The peripheral ligands with pyridine and 2,3-dihydrobenzo [b] thiophene were used to synthesize two series of complexes with different lengths and anchoring groups. The electrochemical and single molecular conductance properties of these two series of ruthenium complexes were studied experimentally by employing cyclic voltammetry and the scanning tunnelling microscopy-break junction technique (STM-BJ) and theoretically using density functional theory (DFT).

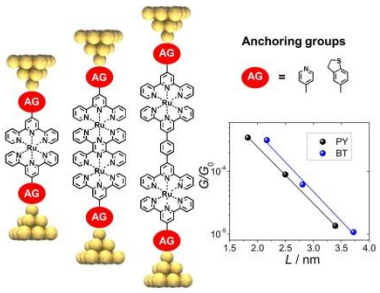

Hiroaki Ozawa, Masoud Baghernejad, Oday A. Al-Owaedi, Veerabhadrarao Kaliginedi,* Takumi Nagashima, Jaime Ferrer, Thomas Wandlowski, Víctor M. García-Suárez, Peter Broekmann, Colin J. Lambert and Masa-aki Haga**

Page No. – Page No.

Synthesis and Single-Molecule Conductance study of Redox Active Ruthenium Complexes with Pyridyl and Dihydrobenzo[b]thiophene Anchoring Groups